

Article

Harmonic Loss Analysis of Low-Voltage Distribution Network Integrated with Distributed Photovoltaic

Wenqian Yuan ¹, Xiang Yuan ², Longwei Xu ^{3,*}, Chao Zhang ¹ and Xinsheng Ma ¹¹ State Grid Jibei Electric Power Research Institute, Beijing 100045, China² State Grid Jibei Electric Power Company Limited, Beijing 100053, China³ School of Electrical Engineering, Shandong University, Jinan 250061, China

* Correspondence: 202034717@mail.sdu.edu.cn

Abstract: In a power system with highly proportional renewable energy integration, the power generated by photovoltaic (PV) of high permeability and high proportion needs to be connected to the distribution network through the power electronic inverter. The inverters can generate the low-order harmonic and high-order harmonic near the switching frequency. Harmonic power will be generated when the harmonic current flows through the power grid with the harmonic voltage of the same frequency, and the additional harmonic losses caused should not be neglected. To effectively analyze the voltage quality and calculate the harmonic loss of the low-voltage distribution network integrated with distributed PV, based on the harmonic loss factor of resistance proposed, the harmonic impedance modeling and harmonic loss calculation method for the key equipment of the power grid, such as lines and transformers, are introduced in this paper firstly. Next, a decoupling algorithm of harmonic power flow is proposed, and the influence of the access capacity of PV on voltage quality and line loss of the distribution network is analyzed. Finally, a harmonic loss calculation method based on measured harmonic data of the distribution network is proposed. It is found that the harmonic loss of the low-voltage distribution network accounts for about 0.6% of the total network loss. Therefore, voltage quality can be improved and line loss can be reduced effectively by reasonable access to PV and reducing harmonic order and the current harmonic distortion.

Keywords: distributed PV; distribution network; harmonic loss; measured data

Citation: Yuan, W.; Yuan, X.; Xu, L.; Zhang, C.; Ma, X. Harmonic Loss Analysis of Low-Voltage Distribution Network Integrated with Distributed Photovoltaic. *Sustainability* **2023**, *15*, 4334. <https://doi.org/10.3390/su15054334>

Academic Editors: Pedro Dinis Gaspar, Pedro Dinho da Silva and Luís C. Pires

Received: 5 January 2023

Revised: 8 February 2023

Accepted: 27 February 2023

Published: 28 February 2023



Copyright: © 2023 by the authors. Licensee MDPI, Basel, Switzerland. This article is an open access article distributed under the terms and conditions of the Creative Commons Attribution (CC BY) license (<https://creativecommons.org/licenses/by/4.0/>).

1. Introduction

With carbon peak and carbon neutrality goals, the renewable energy generation technology represented by photovoltaic (PV) is widely considered [1,2]. Because of clean and sufficient solar energy resources and convenient installation methods, such as “roof photovoltaic”, the economic and environmental benefits of the PV generation system are continuously improved [3,4]. When a high proportion of distributed energy is connected to the power grid, the change in configuration and operation condition of the distribution network is huge [5] and the power flow of the distribution network has significantly been changed [6,7]. On the one hand, distributed PV will affect the power flow of the distribution network, directly affecting the loss of lines and equipment [8]. On the other hand, the randomness and intermittence of PV output power will bring a series of problems, such as harmonics [9,10]. The interaction with the original power quality disturbance factors further complicates the power quality disturbance mechanism of the distribution network, indirectly increasing the complexity of distribution network loss analysis [11] and the difficulty of reducing loss [12]. Therefore, it is of great significance to study the influence mechanism of the network loss of the distribution network integrated with a high proportion of distributed PV.

PV needs to be connected to the distribution network through power electronic inverters [13], resulting in various low-frequency harmonics and high-frequency harmonics

near the switching frequency [14,15]. Non-ideal factors of the inverter, such as the accumulation of dead time, cause low-order harmonics. The delay characteristics of sinusoidal pulse width modulation (SPWM) will produce high-frequency harmonics [16]. At present, there are various types of inverters. Their operation control and non-ideal characteristics of the access terminal will bring harmonic distortion to the distribution network [17,18]. Harmonics caused will reduce the insulation level and life of transformers, cables and other equipment, and increase copper, iron and dielectric losses [19]. Therefore, harmonics should be analyzed in the distribution network with PV integration.

Harmonic power flow calculation is an important basis for harmonics research [20] and an important means to understand the harmonic characteristics of the power grid and analyze harmonics [21,22]. In order to analyze the harmonic power flow, the constant current source model is widely used in engineering [23]. The phase angle of the typical spectrum in the constant current source model is determined by experiment or simulation [24]. At the same time, this method is only applicable to the analysis of a single harmonic source in the system [25]. With large-scale PV integration, the system contains multiple harmonic sources, and, thus, the iterative harmonic power flow becomes effective. In iterative harmonic analysis, the harmonic current of the harmonic source is a variable controlled by its terminal voltage [26]. Newton–Raphson or Gauss methods are used to update the terminal voltage of harmonic sources, and harmonic currents are solved by alternating iterations [27]. Convergence performance and computation speed are the main factors affecting the application of this method. The unified harmonic power flow method using the Newton–Raphson method can solve the fundamental and harmonic power flows. The deviation equation and Jacobi matrix are simplified, so the calculation speed and convergence are improved [28]. The current source direct solution method also is a harmonic power flow analysis method. It is widely used in engineering, and the decoupling method is further simplified. Ignoring the influence of harmonic power flow on the fundamental power flow, the fundamental and harmonic power flows are solved separately. Only the influence of the fundamental voltage of the bus on the harmonic injection current is considered [29]. However, the phase angle estimation of harmonic current is not accurate. Therefore, the interaction between multiple harmonic currents cannot be considered when multiple harmonic sources exist in the system.

At present, the influence of harmonics on the active power loss of the low-voltage distribution network has been studied by a large number of papers. In [30], the influence of harmonics on the loss is analyzed, the Norton equivalent method is used to model the nonlinear load of the distribution network and it is verified that the power loss of the distribution network caused by harmonic distortion can be as high as 20%. In [31], a novel harmonic model of the three-phase transformer is proposed. The skin effect and proximity effect of transformer windings under harmonic background are considered in this model. The harmonic loss of the transformer is accurately calculated by using the hysteresis model. In [32], the skin effect and hysteresis and eddy current loss of the stranded wire are considered, and the relative resistance increment caused by the skin effect of the stranded wire is calculated. At the same time, it is not suitable for approximate calculation in engineering, owing to a large number of parameters and complex calculation processes. The existing references are all theoretical studies on the influence of harmonics on single equipment [33], and the proportion of line loss caused by harmonics was not specifically quantified.

To systematically and quantitatively analyze the harmonic loss, a harmonic loss calculation method for the low-voltage distribution network integrated with distributed PV based on measured data is proposed in this paper. The contributions of the paper are as follows:

- (1) The harmonic impedance modeling and harmonic loss calculation methods for the key equipment of the power grid, including lines and transformers, are introduced, and the quantitative relationship between harmonic current content and harmonic order and harmonic loss is obtained.

- (2) The fundamental power flow is solved iteratively by the Newton method, and the harmonic power flow is solved by the decoupling algorithm. The influence of PV capacity on voltage quality and line loss is analyzed.
- (3) The harmonic loss calculation method based on the measured harmonic data of the low-voltage distribution network is proposed.

The rest of the paper is organized as follows. Section 2 analyzes the operation mechanism of the distributed PV system. Section 3 describes the equipment loss model considering harmonic factors. Section 4 illustrates the harmonic power flow algorithm. Section 5 presents the simulation analysis and Section 6 summarizes the study's conclusions.

2. Operation Mechanism of Distributed PV System

2.1. PV Generation Model

The distributed PV is mainly based on solar cells, which can convert solar energy into DC energy. A simplified circuit of the solar cells is shown in Figure 1. In this figure, I_{ph} is the photogenerated current; I_D is the reverse saturation current of the diode; I_p is the leakage current of solar cells; R_p is the parallel resistance; R_s is the series resistance; U_{out} is output voltage; I_{out} is output current.

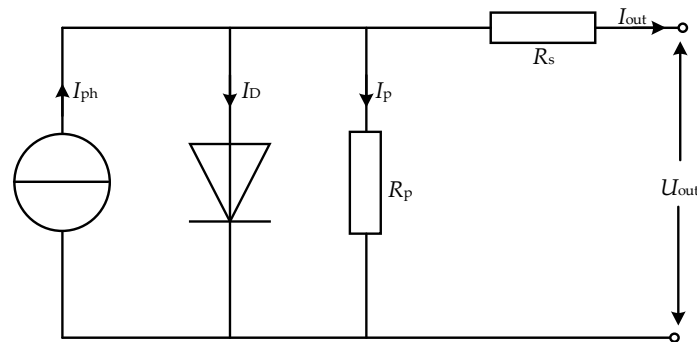


Figure 1. The simplified circuit of the solar cells.

In the simplified circuit, solar cells can be considered equivalent circuits composed of a current source and diode in parallel. The current source simulates the photocurrent and the diode simulates the internal semiconductor material characteristics. The equivalent series resistance R_s is small, which is used to simulate the body resistance of the material and the contact resistance of the electrode. Because PV cells have a certain leakage current, the equivalent parallel resistance R_p is used to simulate the leakage loss. According to Kirchhoff's current law, it can be formulated as:

$$I_{out} = I_{ph} - I_D - I_p \quad (1)$$

$$I_p R_p = U_{out} + I_{out} R_s \quad (2)$$

The conduction current equation of the diode is:

$$I_D = I_0 \left\{ \exp \left[\frac{q(I_{out} R_s + U_{out})}{AKT} - 1 \right] \right\} \quad (3)$$

where I_0 is the reverse saturation current of the diode; K denotes the Boltzmann constant, and its value is 1.38×10^{-23} J/K; T is Kelvin thermodynamic temperature; and q represents a unit of electric quantity, and its value is 1.6×10^{-19} C. Therefore, the output current of solar cells is:

$$I_{out} = I_{ph} - I_0 \left\{ \exp \left[\frac{q(I_{out} + U_{out})}{AKT} - 1 \right] \right\} - \frac{U_{out} + I_{out} R_s}{R_p} \quad (4)$$

The DC cannot be directly provided to users. It is necessary to convert the DC power into AC power with frequency and amplitude matching the grid through the inverter part [34]. The structure of the PV grid-connected is shown in Figure 2. The voltage source inverter by PWM control is used in the main circuit. The voltage and current double closed-loop control is used as the control mode [35]. The output AC power of the inverter part contains more harmonics, especially high-frequency harmonics, which cannot be directly incorporated into the power grid. The filter is installed to filter out harmonic current at the AC side of the inverter. At present, the commonly used filters are L-, LC- and LCL-types. The LCL-type filter is widely used because of its superior high-frequency harmonic suppression ability without large inductance. It also has good performance and a low price.

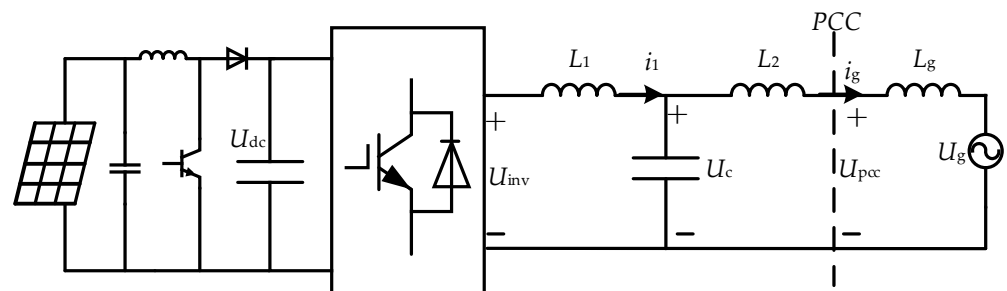


Figure 2. The structure of the PV grid-connected.

2.2. Harmonic Generation Mechanism

There are many unsatisfactory factors of the PV inverter. For example, the low-frequency harmonics are generated by the accumulation of dead time, and the high-frequency harmonics are generated by the switching characteristics of sinusoidal pulse width modulation. At the same time, the inverter types are different and various, and their operation control and non-ideal characteristics will bring harmonic distortion to the distribution network. The distributed integration of PV with high permeability results in high harmonic distortion, strong randomness and wide harmonic frequency coverage, which increases the copper, iron and dielectric losses of equipment and reduces the insulation level and service life of transformers and cables.

To ensure the normal operation of the switching device, the dead time must be added to the power electronic switching device. However, the zero current clamping effect is produced and the low harmonic distortion of inverter output increases. The error voltage expression is:

$$U_{Tdn} = \frac{4f_c T_d U_{dc}}{n\pi} \sin n(\omega_r t - \varphi), n = 3, 5, 7, \dots \quad (5)$$

where U_{dc} is the DC voltage of the PV inverter; f_c is carrier frequency; n is harmonic order relative to modulated wave; φ is the initial phase of the modulated wave; T_d is dead time. According to the equation, the harmonic will also increase with the increase of dead time, DC voltage and carrier frequency. The order of harmonic voltage caused by the dead time effect is $6k \pm 1, k = 1, 2, 3, \dots$, so the 5th, 7th, 11th et al. odd harmonic voltage can be obtained by Fourier decomposition.

The working mechanism of the inverter determines that SPWM modulation will produce high-frequency harmonics. With bipolar SPWM modulation, the inverter output line voltage U_{ab} can be obtained. By Fourier decomposition, the fundamental voltage component U_{ab1} is:

$$U_{ab1} = \frac{\sqrt{3}}{2} m U_{dc} \sin\left(\omega_r t + \varphi + \frac{\pi}{3}\right) \quad (6)$$

where m is the harmonic order of carrier u_c .

The carrier angular frequency is ω_c , and the modulation wave angular frequency is ω_r . When the frequency is $n\omega_r \pm k\omega_c$, the harmonic components U_{abn} can be expressed as follows.

(1) When $n = 1, 3, 5, \dots, k$ is even other than an integer multiple of 3.

$$U_{abn} = \sum_{m=1}^{\infty} (-1)^{\frac{m+1}{2}} \frac{4U_{dc}}{m\pi} \sum_{n=2}^{\infty} J_n\left(\frac{m\pi M}{2}\right) \sin\left[(m\omega_c \pm n\omega_r)t + n\left(\varphi - \frac{\pi}{3}\right)\right] \sin \frac{n\pi}{3} \quad (7)$$

(2) When $n = 2, 4, 6, \dots, k$ is odd other than an integral multiple of 3.

$$U_{abn} = \sum_{m=2}^{\infty} (-1)^{\frac{n}{2}} \frac{4U_{dc}}{m\pi} \sum_{n=1}^{\infty} (-1)^n J_n\left(\frac{m\pi M}{2}\right) \cos\left[(m\omega_c \pm n\omega_r)t + n\left(\varphi - \frac{\pi}{3}\right)\right] \sin \frac{n\pi}{3} \quad (8)$$

where J_n is the Bessel function; n is the harmonic order; M is the degree of modulation. When the degree of modulation $M = 1$, the voltage utilization rate is 0.886, there is no integer multiple harmonic of carrier frequency ω_c and there is no integral multiple harmonic of 3 of the modulated wave frequency ω_r . According to the properties of the Bessel function, its change rule is similar to that of the trigonometric function. The amplitude of each harmonic is related to the degree of modulation M . As the carrier ratio increases, the amplitude of the harmonic voltage increases or decreases. When appropriate filtering schemes and control methods are used, specific frequency harmonics can be eliminated or reduced.

In practice, a distributed PV system usually works in the “full access” power supply mode. In addition to the inevitable characteristic harmonics caused by the normal operation and pulse modulation of the PV inverter, the output current of the PV inverter also contains interharmonics. Changes in light intensity and temperature lead to changes in PV output power, and interharmonics are generated in the grid. A PV grid-connected system using a maximum power point tracking strategy will cause the DC voltage command value to fluctuate. Rich interharmonic currents are generated in the grid through the interaction of harmonics/interharmonics on the AC/DC side of the inverter. In addition, the voltage background interharmonics at the PV grid connection point can cause it to inject interharmonic currents into the grid. ω_m is the interharmonic angular frequency of the DC side, and the harmonic frequency of the AC side will be shifted by $\pm\omega$.

2.3. Influence of PV Output Power on Harmonic Characteristics

The vector diagram of the grid-connected inverter under the steady-state condition is shown in Figure 3. In this figure, U_s is the effective value of phase voltage on the AC side; I is the grid-connected current; φ is the power angle factor; U_{inv} is the output phase voltage effective value of the inverter; ω_1 is the fundamental frequency of the power grid.

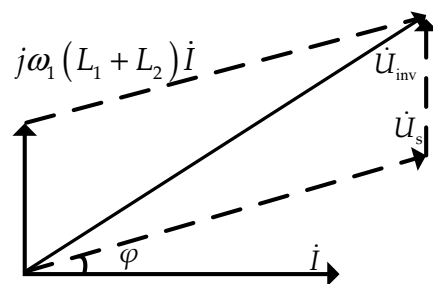


Figure 3. The steady-state vector diagram of the grid-connected inverter.

The capacitance current of the filter at the fundamental frequency is small and can be ignored. If the active power of the PV inverter output is P_{pv} and the reactive power is Q_{pv} , the effective value of the grid current is:

$$I = \frac{\sqrt{P_{pv}^2 + Q_{pv}^2}}{3U_s} \quad (9)$$

The output voltage effective value of the inverter U_{inv} is:

$$U_{inv} = \frac{MU_{dc}}{2\sqrt{2}} \quad (10)$$

According to the law of cosines:

$$I^2(\omega_1 L_1 + \omega_1 L_2)^2 + U_s^2 + 2IU_s(\omega_1 L_1 + \omega_1 L_2) \sin \varphi = U_{inv}^2 \quad (11)$$

Therefore, it can be obtained that:

$$M = \frac{2\sqrt{2}}{U_{dc}} \sqrt{\frac{P_{pv}^2 + Q_{pv}^2}{9U_s^2} (\omega_1 L_1 + \omega_1 L_2)^2 + \frac{2}{3} Q_{pv} (\omega_1 L_1 + \omega_1 L_2) + U_s^2} \quad (12)$$

The change in the degree of modulation is positively related to the change of output power, so the PV output power affects the output harmonic amplitude of the inverter.

3. Equipment Loss Model Considering Harmonic Factors

3.1. Calculation Model of Line Harmonic Loss

The influencing factors of line harmonic loss are the magnitude of harmonic current and harmonic resistance. Harmonic current is related to the operation characteristics of the power grid. Under the harmonic background, the line resistance is affected by the harmonic order and line skin effect. The influence of the proximity effect, the hysteresis and eddy current of the steel core and the protection of the steel strip also should be considered.

Without considering the influence of harmonics on the impedance of transmission lines, the line harmonic loss of the distribution network can be expressed as:

$$P_w = 3I^2R = 3(I_1^2 + \sum_{n=2}^M I_n^2)R = 3I_1^2R(1 + \frac{\sum_{n=2}^M I_n^2}{I_1^2}) = 3I_1^2R(1 + THD_I^2) \quad (13)$$

where I is the sum of fundamental current and harmonic current; R is line equivalent resistance; I_1 is fundamental current; I_n is n th harmonic current; THD_I is the total harmonic distortion of current; M is the highest harmonic order. The loss increase rate of distribution network lines is the ratio of the loss generated by harmonics to the loss of fundamental current:

$$\alpha = \frac{I^2R - I_1^2R}{I_1^2R} = THD_I^2 \quad (14)$$

In practice, the impedance of the line changes with the harmonic frequency, especially when the harmonic frequency is higher. Wakileh et al. proposed that with the increase of the frequency, the skin effect becomes more obvious, and the current in the conductor concentrates on the surface, resulting in an increase in AC resistance and a decrease in internal resistance and inductance. Considering the skin effect under harmonic conditions, the impedance of the conductor is:

$$Z(n) = \sqrt{n}(R + jX) \quad (15)$$

The harmonic loss of the line of the simplified model can be expressed as:

$$P_{loss} = 3 \sum_{n=2}^M I_n^2 R_n = 3I_1^2 R_1 \sum_{n=2}^M \sqrt{n} (HRI_n)^2 \quad (16)$$

where R_1 is line fundamental frequency resistance; HRI_n is the ratio of harmonic current to fundamental current. The effects of permeability, conductor radius and conductivity are neglected in this method. The calculation results may be quite different from the actual ones.

The calculation standard JCS 0374 for bare wire carrying capacity was published by Japan Wire Industry Association [36]. The AC/DC resistance coefficient is introduced through the AC/DC resistance test of wire:

$$k = R_{AC}/R_{DC} = k_1 \times k_2 \quad (17)$$

where R_{AC} is AC resistance; R_{DC} is DC resistance; k_1 is the skin effect coefficient; k_2 is the core loss coefficient. Formula (17) shows the AC/DC resistance ratio at different frequencies. The skin effect of the conductor and the iron loss caused by hysteresis and the eddy current of the steel core are considered. k_1 can be written as:

$$k_1 = a + bx - cx^2 + dx^3 \quad (18)$$

where $a = 0.99609$; $b = 0.18578$; $c = -0.030263$; $d = 0.020735$. For single strand (aluminum alloy wire and aluminum alloy core wire), x can be written as:

$$x = 0.01 \sqrt{8\pi f / R_{DC}} \quad (19)$$

For composite wire (aluminum wire and steel wire), x can be written as:

$$x = \frac{(D_1 + 2D_2)}{D_1 + D_2} \sqrt{\frac{80\pi f (D_1 - D_2)}{(D_1 + D_2)R_{DC}}} \times 10^{-4} \quad (20)$$

where f is frequency; D_1 is the outer diameter of the strand; D_2 is the outer diameter of steel wire. For the single strand and composite strand (the number of aluminum wire layers is even), the iron loss coefficient $k_2 = 1$. For composite strands (more than 1 odd number of aluminum layers), k_2 can be written as:

$$k_2 = a + by - cy^2 + dy^3 \quad (21)$$

s.t. $y = I/A$

where $a = 0.99947$; $b = 0.028859$; $c = -0.0059348$; $d = 0.00042259$; I is stranded wire current; A is section area of aluminum wire. If the values of k_1 and k_2 are less than 1, $k_1 = 1$ and $k_2 = 1$. This method has comprehensive factors and relatively simple calculation, which is more suitable for AC resistance calculation under harmonic background. Therefore, the loss power of the n th harmonic of the line can be written as:

$$P_n = k \cdot I_n^2 R_{DC} \quad (22)$$

3.2. Calculation Model of Transformer Harmonic Loss

Distribution transformer loss mainly has two parts, which are copper loss and iron loss. The excitation branch of the transformer is nonlinear due to the existence of the iron core, and its nonlinearity varies with the applied voltage. The higher the voltage is, the closer the core is to saturated, and the greater the degree of nonlinearity is. When the applied voltage is not high, the core is not saturated, and the voltage harmonic distortion is not large. Therefore, the influence of harmonics on the iron loss of the transformer can be ignored. Without considering the influence of harmonics on the excitation branch of the distribution transformer, the harmonic equivalent circuit of the distribution transformer is shown in Figure 4.

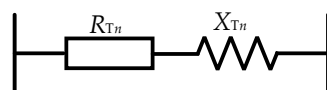


Figure 4. The harmonic equivalent resistance of the transformer.

The impedance is composed of the winding resistance and leakage reactance of the transformer, and the inductance in the leakage reactance is often approximated as a constant. Therefore, the leakage reactance of the transformer X_{Tn} is the product of the fundamental frequency reactance and the harmonic order, which can be expressed as:

$$X_{Tn} = nX_{T1} \quad (23)$$

where X_{T1} is the fundamental frequency reactance of the transformer. When there are harmonics in the transformer, due to the skin effect and proximity effect, the resistance of the winding will increase. It is usually considered to be proportional to the square root of the harmonic order. Therefore, the harmonic impedance formula of the simplified model can be expressed as:

$$Z_{Tn} = \sqrt{n}R_{T1} + jnX_{T1} \quad (24)$$

where R_{T1} is the fundamental frequency winding resistance of the transformer. This method is suitable for the simple estimation of harmonic line loss in engineering practice, and there will be a large error when there are high-frequency harmonics in the system.

Under the harmonic background, due to the winding skin effect, the resistance of the transformer has the following relationship with the harmonic order [37]:

$$R_n = R_1(c_0 + c_1n^b + c_2n^2) \quad (25)$$

c_0 , c_1 , c_2 and b are coefficients, which are related to the material and length of winding. Generally, $c_0 + c_1 + c_2 = 1$. The value range of each coefficient is shown in Table 1 [37].

Table 1. The value range of each coefficient.

	C_0	C_1	C_2	B
distribution transformer	0.85~0.90	0.05~0.08	0.05~0.08	0.9~1.4
power transformer	0.75~0.80	0.10~0.13	0.10~0.13	0.9~1.4

Harmonic loss of transformers can be expressed as:

$$P_{LL} = 3K \cdot \sum_{n=2}^M I_n^2 R_1 (c_0 + c_1 n^b + c_2 n^2) \quad (26)$$

where K is the constant coefficient. This method is simple to calculate, and fewer factors are considered. The eddy current and stray loss under harmonic conditions are not considered. In addition, because the constant coefficient in Formula (26) is not fixed, it is related to artificial selection, and the calculation error is large.

The transformer load loss is divided into DC loss, winding eddy current loss and other stray losses in IEEE/ANSI C57.110 standard [38]. Among them, the winding resistance loss is the main part of the loss, accounting for about 80% of the loss. The loss of the winding eddy current accounts for about 33% of the additional loss. The winding eddy current harmonic factor F_{HL-EC} and other stray loss harmonic factor F_{HL-OSL} are used to calculate the additional loss of the transformer under harmonics. They can be expressed as:

$$F_{HL-EC} = \frac{\sum_{n=1}^M I_n^2 n^2}{\sum_{n=1}^M I_n^2} = \frac{\sum_{n=1}^M \left[\frac{I_n}{I_1} \right]^2 n^2}{\sum_{n=1}^M \left[\frac{I_n}{I_1} \right]^2} \quad (27)$$

$$F_{\text{HL-OSL}} = \frac{\sum_{n=1}^M I_n^2 n^{0.8}}{\sum_{n=1}^M I_n^2} = \frac{\sum_{n=1}^M \left[\frac{I_n}{I_1} \right]^2 n^{0.8}}{\sum_{n=1}^M \left[\frac{I_n}{I_1} \right]^2} \quad (28)$$

Considering the effect of skin effect on winding resistance under harmonic current, the harmonic loss factor of winding resistance $F_{\text{HL-R}}$ is defined as

$$F_{\text{HL-R}} = \frac{\sum_{n=1}^M I_n^2 n^{0.5}}{\sum_{n=1}^M I_n^2} = \frac{\sum_{n=1}^M \left[\frac{I_n}{I_1} \right]^2 n^{0.5}}{\sum_{n=1}^M \left[\frac{I_n}{I_1} \right]^2} \quad (29)$$

The total transformer loss under harmonic background can be expressed as:

$$P_T = P_{\text{NL}} + (F_{\text{HL-R}} P_R + F_{\text{HL-EC}} P_{\text{EC-R}} + F_{\text{HL-OSL}} P_{\text{OSL-R}}) \cdot \left(\frac{I}{I_R} \right)^2 \quad (30)$$

where P_{NL} is fixed loss; P_R , $P_{\text{EC-R}}$ and $P_{\text{OSL-R}}$ are resistance loss, winding eddy current loss and other stray loss under rated operating conditions. It can be found that the loss is mainly determined by the secondary side current. The effect of skin effect on transformer winding resistance is considered, and the winding resistance loss is calculated in Formula (13). It is more accurate than the calculation method proposed in IEEE Std C.57.110.

4. Harmonic Power Flow Calculation Model of Distribution Network

Fundamental power flow and harmonic power flow are decoupled by the decoupling method in the harmonic power flow analysis. In the analysis of fundamental power flow, the influence of harmonics is not considered, and the fundamental voltage and current are obtained independently. Based on the voltage and current of the fundamental power flow, the harmonic solution is realized by combining the harmonic source model and the harmonic network equation. The calculation process of harmonic power flow is simplified, and the accuracy of the results are satisfactory by this method. The calculation steps are as follows.

Step 1: The solution of fundamental voltage and fundamental power flow is realized based on the fundamental power flow equation. The fundamental power flow equation is as follows:

$$\begin{cases} P_i = V_i \sum_{j=1}^n V_j (G_{ij} \cos \delta_{ij} + B_{ij} \sin \delta_{ij}) \\ Q_i = V_i \sum_{j=1}^n V_j (G_{ij} \sin \delta_{ij} - B_{ij} \cos \delta_{ij}) \end{cases} \quad (31)$$

where the subscript is the node number; P_i and Q_i are fundamental active and reactive power; V_i and V_j represent the node voltage amplitudes; G_{ij} and B_{ij} are conductance and susceptance parameters of the line; δ_{ij} represents the phase angle difference of node voltage. The traditional Newton–Raphson method is usually used to solve the fundamental power flow in the distribution network, and the fundamental voltage data of the harmonic source node are obtained.

Step 2: The harmonic source model of PV is established. In general, the harmonic distortion of each node voltage is less than the limit value specified in the national standard, and the harmonic voltage is far less than the fundamental voltage in numerical value. The effect of harmonic voltage on harmonic injection current is also very small, which can be approximately ignored. Therefore, the harmonic source is regarded as a harmonic constant current source with infinite internal impedance. The amplitude and phase angle of har-

monic current depends on the typical frequency spectrum of harmonic source equipment. It can be expressed as:

$$\begin{cases} I_h = I_f \frac{I_{h,\text{spectrum}}}{I_{f,\text{spectrum}}} \\ \theta_h = \theta_{h,\text{spectrum}} + h(\theta_f - \theta_{f,\text{spectrum}}) \end{cases} \quad (32)$$

where I_h and θ_h are h th harmonic current amplitude and phase angle; I_f and θ_f are the magnitude and phase angle of fundamental current; $I_{h,\text{spectrum}}$ and $\theta_{h,\text{spectrum}}$ are the spectrum values of the h th harmonic current magnitude and phase; $I_{f,\text{spectrum}}$ and $\theta_{f,\text{spectrum}}$ are the spectrum values of the fundamental current magnitude and phase.

Step 3: To solve the harmonic current of the network, it is necessary to obtain the network equation of the system under harmonic frequency in harmonic power flow analysis. Therefore, generators, lines, transformers and linear loads need to be modeled. The specific process is shown in Appendix A.

Step 4: According to the fundamental power flow data and harmonic source model, the h th harmonic current matrix I_h is obtained. Based on the nodal admittance matrix Y_h and its inverse matrix Z_h under a certain harmonic order, the solution of harmonic voltage matrix V_h is obtained.

$$\begin{cases} I_h = Y_h V_h \\ V_h = Z_h I_h \end{cases} \quad (33)$$

Step 5: If the maximum deviation of voltage amplitude of the node i in the k th iteration is smaller than ε (ε is 10^{-7} in this paper) in Formula (34), the iteration can be stopped and the ultimate harmonic voltages are yielded

$$e = \max(|V_i^{(k)}(h) - V_i^{(k-1)}(h)| | i \in N) < \varepsilon \quad (34)$$

Otherwise, the harmonic source is updated, and the above process is repeated until the calculation results converge. N is a collection of node numbers. $V_i^{(k)}(h)$ and $V_i^{(k-1)}(h)$ are the harmonic voltage of this iteration and the harmonic voltage of the previous iteration.

Step 6: Calculating the active power loss of branch ij .

$$P_{ij} = \sum_{i=1}^n \sum_{j=1}^n \left(V_{(h)i}^2 G_{(h)ij} + V_{(h)j}^2 G_{(h)ij} + 2V_{(h)i} V_{(h)j} \cos \theta_{(h)ij} \right) \quad (35)$$

where $V_{(h)i}$ is the h th harmonic voltage of node i .

According to the above solution process, the flow chart of harmonic power flow calculation is shown in Figure 5.

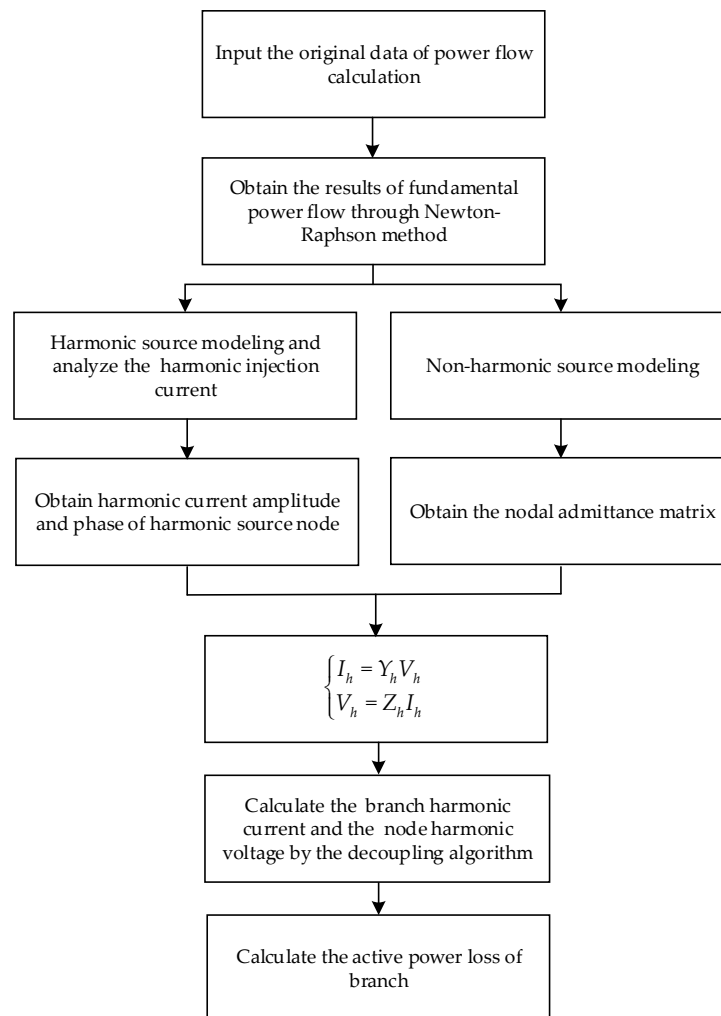


Figure 5. The flow chart of harmonic power flow calculation.

5. Simulation Analysis

In this section, the quantitative relationship between harmonic current content and harmonic order and harmonic loss is analyzed. Then, the influence of the access capacity of PV on voltage quality and line loss of the distribution network is analyzed. Finally, the harmonic loss ratio based on the measured harmonic data of the low-voltage distribution network is calculated. The verification is accomplished using MATLAB 2019a with an Intel i7-10700F CPU and a 16 GB RAM computer.

5.1. Quantitative Analysis of Harmonic Loss in Distribution Network

In the case of harmonics, the line and transformer losses cannot be ignored. According to the line and transformer harmonic line loss model given above, the resistance iron loss coefficient and skin effect coefficient are selected to calculate the line harmonic loss, and the transformer harmonic loss factor is selected to calculate the transformer harmonic load loss. Since the harmonic voltage of the system usually meets the national standard limit, the harmonic loss caused by harmonic voltage is very small compared with the harmonic current. Therefore, this paper focuses on the additional loss caused by the harmonic current. The JLHA2 aluminum-alloy strand with a nominal cross-sectional area of 240 mm² is selected for the distribution line. Its DC resistance is 0.11 Ω/km and the line length is 2.2 km. An S11-200/10 distribution transformer is selected, and the transformer connection group number is Dyn11. Specific parameters are shown in Table 2 [39].

Table 2. Transformer parameters.

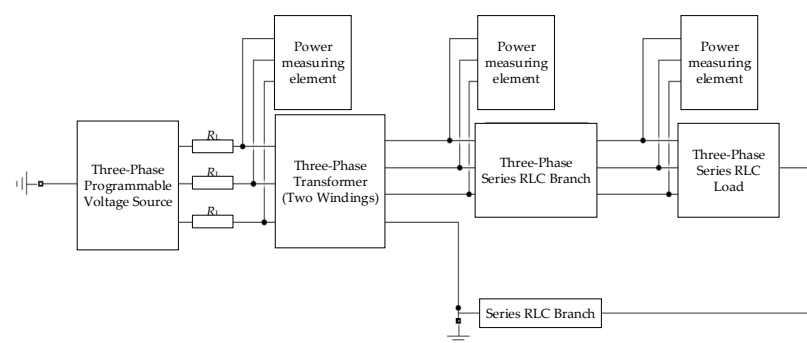
Transformer Parameter	Value
rated capacity/kVA	200
rated voltage/V	10,000/400
no-load loss/W	325
short-circuit loss/W	2600
rated current/A	11.55/288.68
no-load current/%	0.9
impedance voltage/%	4.0

To verify the accuracy of the calculation model of harmonic loss, a simulation model is built in Matlab/Simulink. The parameters of the distribution line and distribution transformer in Matlab are converted. Specific parameters are shown in Table 3.

Table 3. Simulation parameters.

Parameter	Value
resistance of line/ Ω	0.286
inductance of line/mH	5.25
primary resistance of transformer/ Ω	3.25
secondary resistance of transformer/ Ω	0.0052
primary inductance of transformer/H	0.015915
secondary inductance of transformer/mH	0.02546
magnetizing resistance of transformer/ Ω	307692
magnetizing inductance of transformer/H	88.5

The block diagram of the Matlab/Simulink model is shown in Figure 6. The three-phase programmable voltage source is selected to simulate the distribution network system under the background of 7th and 11th harmonics. The electric energy-measuring device consists of the three-phase instantaneous power measuring element and integral link. The loss of the line and transformer are obtained by the difference value of the power meters. To verify the accuracy of the proposed model, the model proposed in this paper (case 1), simplified model (case 2) and simulation results (case 3) are compared in Figure 7.

**Figure 6.** The block diagram of the Matlab/Simulink model.

From the above figure, it can be seen that the simulation result is close to the quantitative calculation result, and the simulation value is slightly larger than the calculated value. Because there are still some differences between the line model and the actual situation, there are always errors between the calculation results and the simulation values of the line, but the error changes little. The error is basically stable at around 4.2%, meeting the requirements of engineering calculation. The calculation error of the transformer increases with the increase of harmonic distortion, but the overall error is not more than 5%. The reason is that the effect of additional iron loss is ignored in the calculation model used in this paper. However, the loss measured by the meter includes additional iron loss caused

by harmonics in the simulation. The errors of the simplified model of the line and the transformer are 20.85% and 55.58%. The above analysis shows that the iron loss increases with the increase of harmonic voltage distortion. In practice, harmonic voltage generally meets the national standard, and this part of loss can be ignored. The effects of permeability, conductor radius and conductivity are neglected in the simplified calculation model, and the calculation results are quite different from the actual ones. The higher the harmonic frequency, the greater the error.

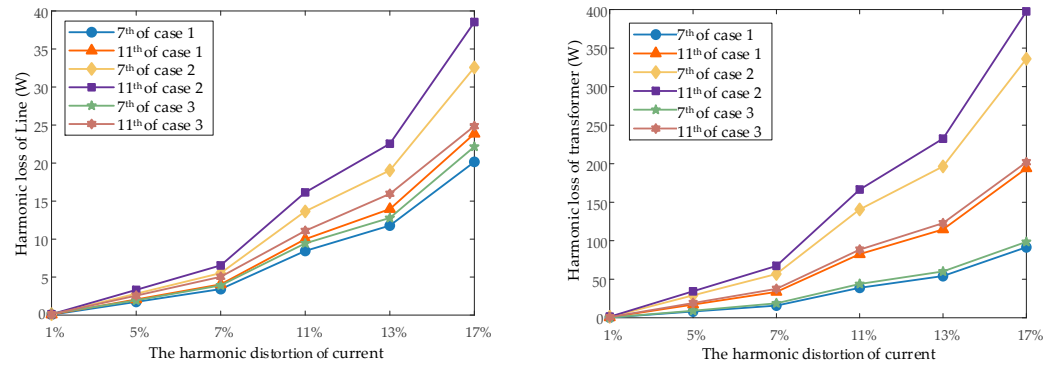


Figure 7. Relationship between the harmonic distortion of current and harmonic loss.

To quantitatively analyze the additional losses of lines and distribution transformers under different harmonic current distortions and different harmonic orders, the 5th, 7th, 11th, 13th and 17th harmonic losses are calculated separately under the condition of 5%, 7%, 11%, 13% and 17% harmonic current distortion of the lines and transformers. The secondary rated current of the distribution transformer is generally used as the fundamental current for the transformer and line. From Formulas (17)–(19), (22) and (27)–(30), the figures of the relationship between harmonic loss of lines and transformers and harmonic distortion and harmonic order are drawn in Figure 8.

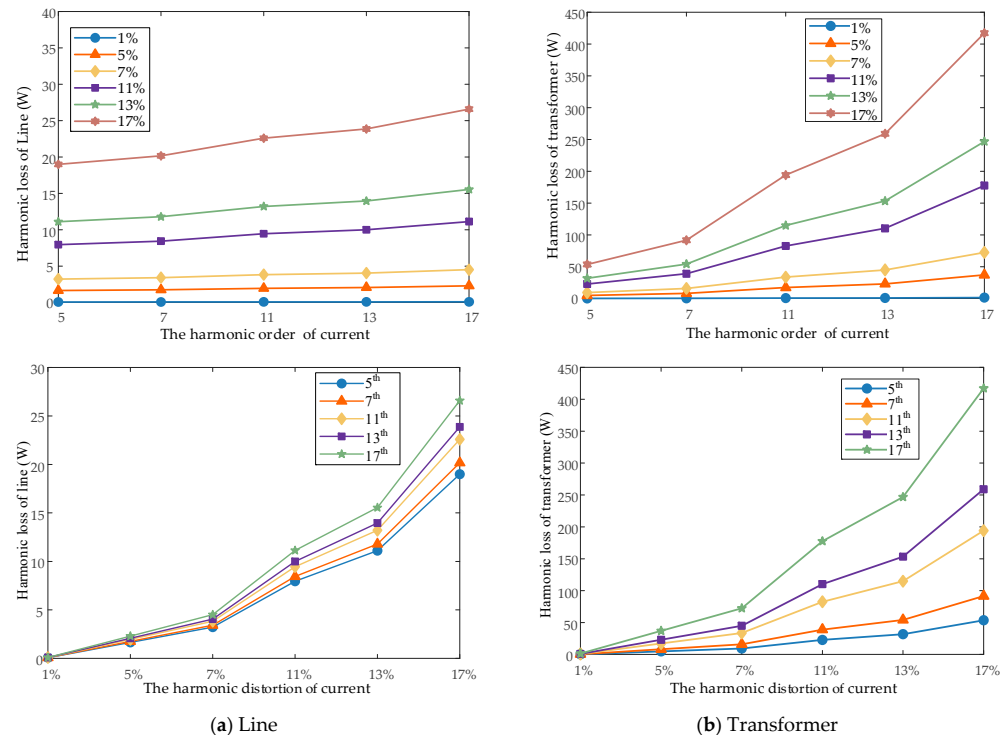


Figure 8. Relationship between the harmonic distortion and harmonic order of current and harmonic loss.

According to the results, when the harmonic order is constant, the line harmonic loss is proportional to the square of harmonic distortion of current, and the higher harmonic of the transformer is approximately proportional to the square of harmonic distortion of current. The harmonic loss of the line is mainly affected by the AC resistance coefficient, and the change is gentle. The harmonic loss of the transformer is mainly affected by the harmonic loss factor and changes rapidly.

When the current harmonic distortion is the same, the higher the harmonic order, the greater the harmonic loss of the low-voltage distribution network. This is because the higher the frequency, the greater the skin effect and proximity effect of the winding and line, so the greater the harmonic impedance of the corresponding transformer and line. Further analysis shows that when the 17th harmonic distortion reaches 17%, the distribution network loss increases by nearly 15%. Therefore, the harmonic has a great influence on the distribution network loss. The copper loss of transformers and transmission line loss increase with the increase of harmonic current content and harmonic order. The proportion of copper loss is much larger than that of line loss and transformer iron loss. Therefore, limiting the content and order of transformer harmonic current is of great significance in reducing branch loss.

5.2. Power Flow Simulation Analysis of Harmonic Loss in Distribution Network

To verify the influence of capacity on network voltage and loss, the impact of distributed PV generation is analyzed. In the MATLAB programming environment, the bus voltage and branch loss of the IEEE 33-bus distribution system are analyzed, and the structure of the IEEE 33-bus system is shown in Figure 9 [40]. The reference voltage of the system is 12.66 kV, and the reference power is 10 MVA, where bus 1 is the balanced node. Distributed PV is connected to bus 16 and bus 33, and the maximum output power of PV is 0.5 MW when the reference light radiation is 1 KW/m².

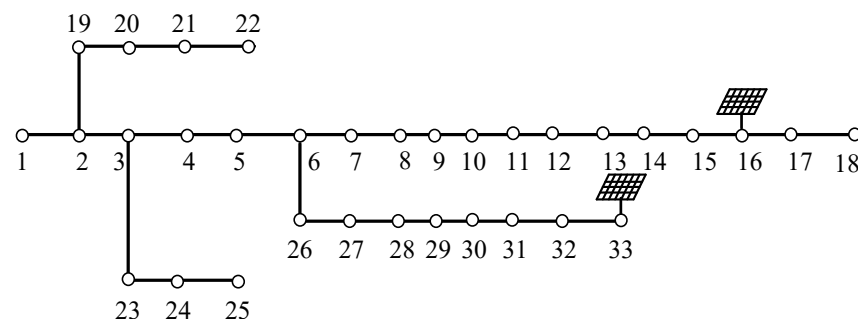


Figure 9. IEEE 33-bus distribution system with PV integration.

The frequency spectrum of harmonics generated by grid-connected PV is shown in Table 4. The load is modeled according to the above harmonic impedance model. High-frequency harmonics are not considered. The low-frequency harmonics generated by grid-connected PV are analyzed, and the highest harmonic order is 7th order. To analyze the fundamental power flow, the PV bus is simplified to the PQ node. The specific parameters of the PV output of each case are listed in Table 5.

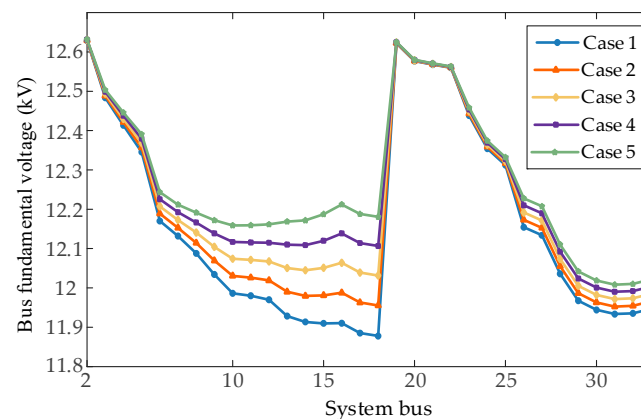
Table 4. Harmonic spectrum of PV generation.

Harmonic Order	Magnitude (%)	Phase (°)
1	100	0
5	19.28	−57.3
7	10.39	−81.13

Table 5. Parameters of PV generation.

Output Conditions	Case 1	Case 2	Case 3	Case 4	Case 5
PV capacity/MW	0.2	0.3	0.4	0.5	0.6

The influence of different PV capacities on fundamental voltage is shown in Figure 10. With the increase of PV permeability, the voltage of each bus also increases. Especially, compared with the bus voltage of the distribution network without PV connection, the maximum rate of change of the bus voltage is 5.37% in Case 5. Therefore, the higher the output power of PV is, the higher the permeability is and the better the supporting effect on the bus voltage is. The above voltage rise is due to the decrease of the equivalent load of the line before the PV access bus, so the voltage drop decreases and the voltage is raised. At the same time, for the branch after the PV access bus, the power flow through the line does not change, so the voltage drop remains unchanged. Due to the front bus voltage being raised, the back bus voltage will also be raised. With the increase of the PV capacity, the change in voltage is greater. Especially in the case of small load demand and large PV output power, the voltage increases significantly.

**Figure 10.** Fundamental voltage variation with different PV capacity access.

From the results in Figure 11, with the increase of PV capacity, the loss of each branch decreases. When the distributed grid-connected PV capacity is in a certain range, the power transmitted by the upper power grid is reduced by increasing the light intensity. The power flowing through the branch is reduced, so the loss of distribution is effectively reduced. Compared with the loss of the distribution network without PV connection, the loss is reduced by 56.26% in Case 5. However, when the access capacity of PV exceeds a certain range, the reverse current of some branches exceeds the forward current without PV access, causing an increase in the network loss.

From Figure 12, with the continuous increase of distributed grid-connected PV capacity on a bus, the harmonic voltage distortion of the whole distribution system increases. In addition, the higher the harmonic frequency is, the more obvious the influence of skin effect on line impedance is, and the greater the influence of harmonic voltage is. The bus with the highest voltage THD is bus 16 in Case 5. The value of the voltage THD is 3.54%. For the PV access bus in the middle and lower reaches of the system, the overall harmonic voltage of the system is greatly affected by PV capacity, especially the voltage of the bus near the PV access bus. Therefore, when distributed PV is connected to the grid, grid-connected PV capacity needs to be controlled within a reasonable range. When the large-capacity distributed PV is connected to the grid, it should be connected by multiple points to reduce the harmonic voltage level of the whole branch.

The resistance of the conductor increases when there are harmonics, and the higher the frequency is, the more obvious the skin effect is and the greater the harmonic resistance is. The harmonic loss of the line increases with the increase of PV capacity and the increase

of the harmonic order in Figure 13. In addition, the 5th harmonic loss accounts for 1.12% of the fundamental loss, and the 7th harmonic loss accounts for 1.30% of the fundamental loss in Case 5. In conclusion, the voltage quality can be effectively improved, and line loss can be reduced through reasonable planning of PV access capacity and reducing harmonic order and harmonic distortion.

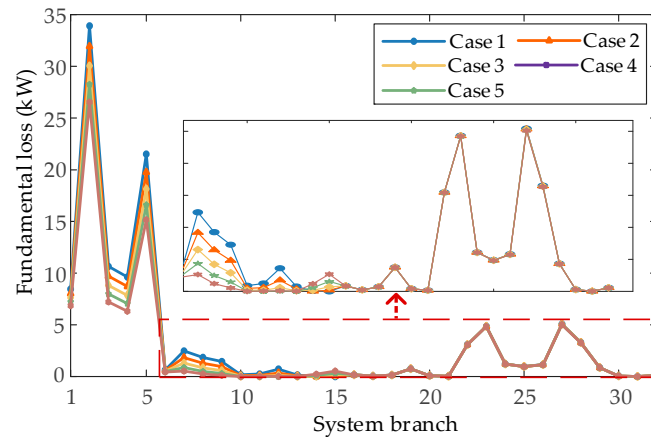


Figure 11. Fundamental loss variation with different PV capacity access.

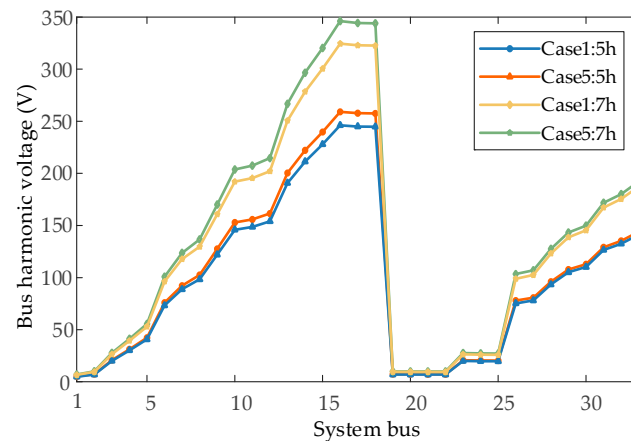


Figure 12. Harmonic voltage variation with different PV capacity access and harmonic order.

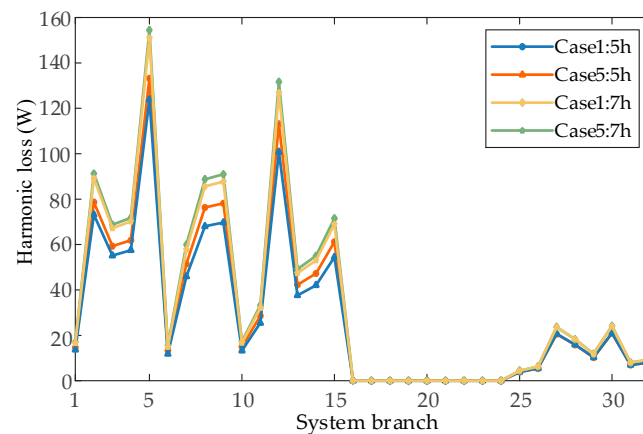


Figure 13. Harmonic loss variation with different PV capacity access and harmonic order.

5.3. Analysis of Measured Data of Low-Voltage Distribution Network

In order to analyze the power quality problems and harmonic losses caused by distributed PV, the measured data are sampled and analyzed. The experimental schematic diagram of the measurement is shown in Figure 14. The data measurement point is the 200 kVA 10 kV/0.4 kV low-voltage outlet side of the transformer, and the distribution network area has five distributed PV accesses. The current and voltage data are sampled by the current transformer and voltage clamp meter. Then, through the data acquisition board and LabVIEW software, the data are input into the computer for analysis and processing. The data characteristics and development rules of the data measurement point are shown as follows.

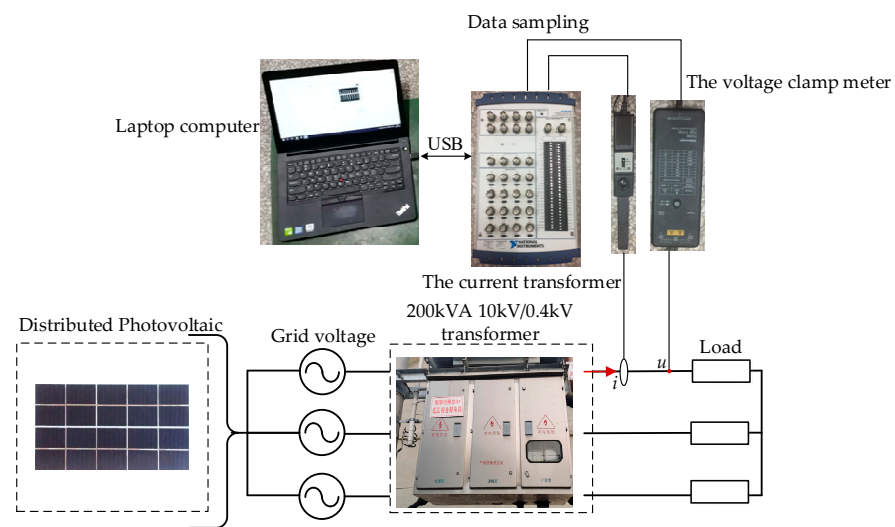


Figure 14. The experimental schematic diagram of the measurement.

The time-varying trends of the fundamental currents of phase A, phase B and phase C in one day are shown in Figure 15. The power generation reaches its peak at noon and is low in the morning and evening. The current of the low-voltage distribution network in the daytime is mainly related to PV output, with a large value. The night current is determined by the user's power load. Therefore, the variation trend of power generation of PV is affected by natural environmental factors such as light intensity and temperature. Taking phase A as an example, the curve of the harmonic current amplitude of phase A varying with time and average and 95th percentile individual demand distortion (IDD) are obtained.

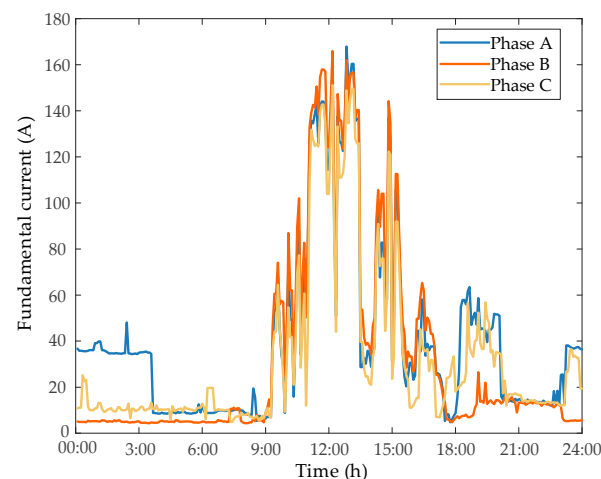


Figure 15. Daily trend of three-phase current.

The time-varying trends of harmonic current in a day are shown in Figure 16. The amplitude of the harmonic current is below 7A, and the harmonic current increases at noon. The harmonic current order of PV output is mainly concentrated in the 5th, 7th and 13th, and the corresponding harmonic distortion decreases with the increase of harmonic order. This is determined by the working characteristics of the 6-pulse PV inverter.

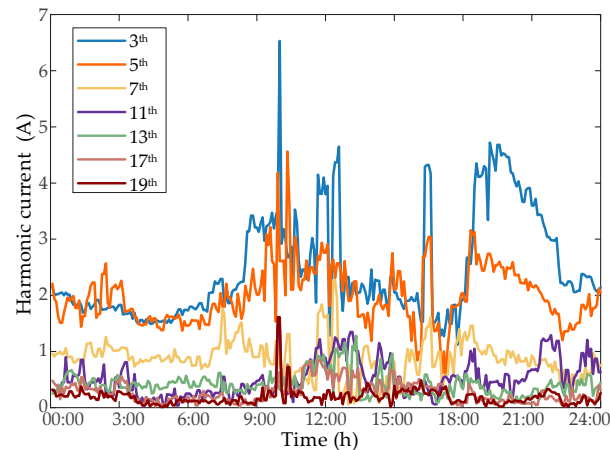


Figure 16. Harmonic current 24-h pattern.

The daily trend of current THD is shown in Figure 17. During the day, PV output power leads to the rapid increase of fundamental current. The change rate of fundamental current is faster than that of harmonic current, so the current THD decreases. The increase of nonlinear load at night and in the morning causes the increase of current THD.

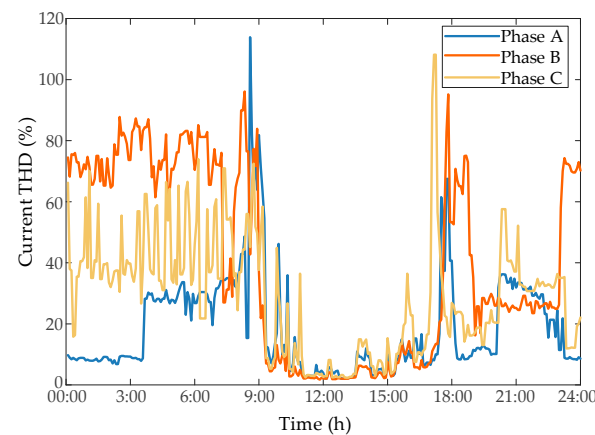


Figure 17. The daily trend of current THD.

In order to analyze the harmonic loss of the station area in one day based on the measured data, a simplified equivalent circuit for the distribution network is shown in Figure 18 [33]. The lines and transformer used in the low-voltage distribution network are the same as the line and transformer selected in Section 3. Based on the measured three-phase voltage, current data of the low-voltage distribution network and the calculation model of harmonic losses of line and transformer proposed in this paper, the percentage of the harmonic loss power of the low-voltage distribution network to the total network loss is obtained.

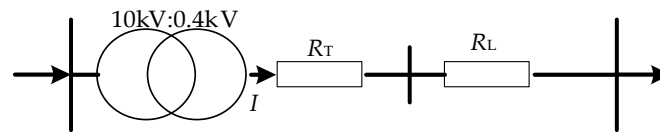


Figure 18. Equivalent circuit of distribution network.

As shown in Figure 19, The time-varying trends of the ratio of harmonic loss power to total loss power are similar to the current THD. It is found that the calculation results are basically consistent with the Matlab simulation results after verification. The ratio is approximately 0.2~1.6%. Taking one day as the statistical period, the branch loss of the station area with the power supply radius of 220 m is 66.7326 kWh, and the harmonic line loss is about 0.399 kWh. The average harmonic loss of the distribution network is about 0.6%. Although the value is small, due to the large loss base of the large-scale low-voltage distribution network, the power loss caused by harmonics is also quite large. Moreover, the harmonic loss power of the low-voltage distribution network is affected by transformer and line type, power supply radius, load rate and harmonic current content rate. Different distribution networks may have different harmonic losses under different operating conditions.

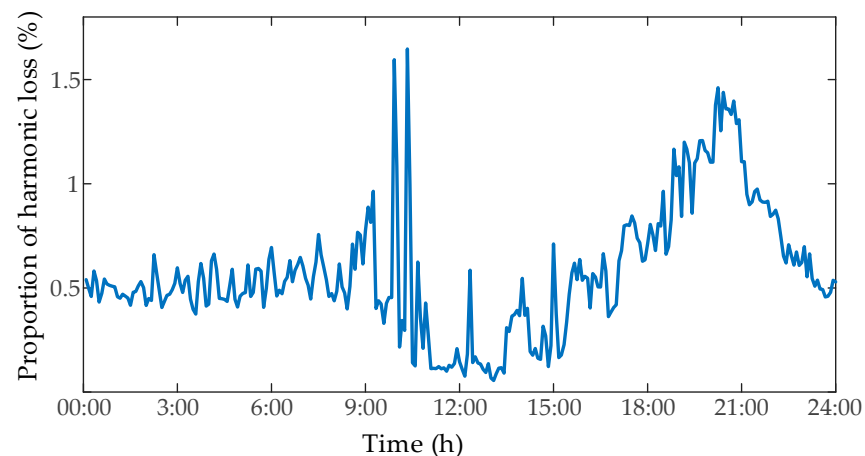


Figure 19. The time-varying trends of ratio of harmonic loss.

To verify the accuracy and reliability of the model and the calculation method, a simple example model is built, as shown in Figure 20.

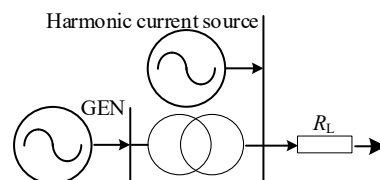


Figure 20. The simple example model.

The comparison between the measurement results and the Matlab simulation results about the harmonic loss of the line are reanalyzed is shown in Figure 4.

From Figure 21, the measurement results are basically consistent with the Matlab simulation results about the harmonic loss of the line. Due to the aging of the line and the loss of measuring instruments, the measurement results are larger than the Matlab simulation results.

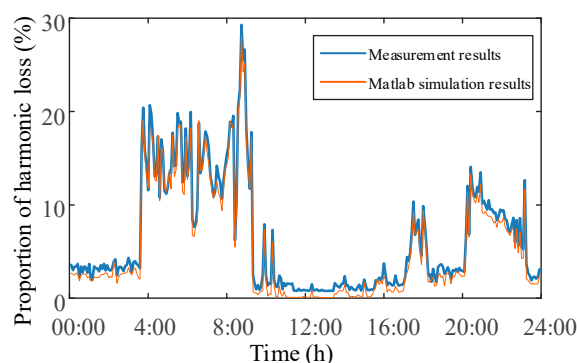


Figure 21. The comparison between the measurement results and the Matlab simulation results.

6. Conclusions

To systematically and quantitatively analyze the harmonic loss of the low-voltage distribution network, the effects of the dead-time effect, SPWM modulation and background harmonics on output harmonic characteristics of PV inverters are studied in this paper. Then, the harmonic loss factor of winding resistance is defined. The harmonic impedance modeling of key equipment such as lines and transformers and the calculation method of harmonic loss of the low voltage distribution network based on measured data are proposed. At last, a harmonic power flow calculation model of the distribution network is presented. The results show that the overall harmonic voltage of the system is greatly affected by PV capacity, especially the voltage of the bus near the PV access bus. In addition, the transformer copper loss and line loss increase with the increase of harmonic current content and harmonic order. It is also found that the harmonic loss of the low-voltage distribution network is mainly determined by the harmonic current, accounting for about 0.6% of the total network loss. Therefore, reasonable planning of PV access capacity and limiting the distortion and order of harmonic current in the low-voltage distribution network is of great significance to reduce network loss.

Author Contributions: Conceptualization, W.Y. and X.Y.; methodology, W.Y.; software, W.Y.; validation, W.Y., X.Y. and L.X.; formal analysis, W.Y.; investigation, W.Y.; resources, W.Y.; data curation, W.Y.; writing—original draft preparation, W.Y.; writing—review and editing, L.X.; visualization, L.X.; supervision, C.Z.; project administration, X.M.; funding acquisition, L.X. All authors have read and agreed to the published version of the manuscript.

Funding: This research received no external funding.

Data Availability Statement: The data presented in this study are available on request from the corresponding author.

Acknowledgments: This work was supported by the State Grid Jibei Electric Power Research Institute under the project of “Upgrading and modification of intelligent control module for distributed PV power quality”.

Conflicts of Interest: The authors declare no conflict of interest.

Appendix A

The generator is modeled in the form of pure reactance. If the reactance of the generator at the fundamental frequency is $X_{G,1}$, then the reactance at h th harmonic frequency can be obtained by the following formula:

$$X_{G,h} = h * X_{G,1} \quad (A1)$$

For dual-winding transformers, the equivalent impedance model can be used. The calculation formula of transformer harmonic impedance Z_{Th} is:

$$Z_{Th} = \sqrt{h} * R_{T1} + j * h * X_{T1} \quad (A2)$$

In power flow calculation, the π -type equivalent circuit can be used as an equivalent harmonic parameter circuit of the line. It is shown in Figure A1.

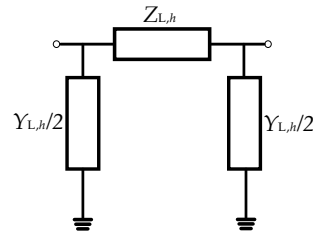


Figure A1. Harmonic parameter model of distribution line.

The parameters in the equivalent circuit are:

$$\begin{cases} Z_{L,h} = Z_{\lambda h} * \sinh \gamma_h l \\ Y_{L,h} = 2 * \frac{\cosh \gamma_h l - 1}{Z_{\lambda h} * \sinh \gamma_h l} \end{cases} \quad (A3)$$

where $Z_{\lambda h}$ is the wave impedance of the line under h th harmonic; λ_h is the propagation constant of the line under h th harmonic; l is the length of the transmission line. Considering that the line length of the distribution network is short, when the harmonic order studied is small, the distribution parameter characteristics are not obvious. The approximate model can be used for analysis. The harmonic impedance $Z_{L,h}$ and ground admittance $Y_{L,h}$ per unit length of the line are shown in Formula (A1).

$$\begin{cases} z_{1,h} = r_{1,h} + h * jx_{1,1} \\ y_{1,h} = h * jb_{1,1} \end{cases} \quad (A4)$$

where $x_{1,1}$ and $b_{1,1}$ are reactance and admittance of line at the fundamental frequency. When the skin effect is considered, the harmonic resistance per unit length can be expressed as:

$$r_{1,h} = 0.288r_{1,1} + 0.138\sqrt{hr_{1,1}} \quad (A5)$$

In harmonic power flow analysis, non-harmonic source load is expressed as an impedance model. If the series impedance model is adopted, the series impedance will be expressed as:

$$\begin{aligned} Z_{L,h} &= R_{L,h} + jX_{L,h} \\ s.t. R_{L,h} &= Re \left(\frac{V_f^2}{\bar{S}_f} \right)^* \\ X_{L,h} &= h * Img \left(\frac{V_f^2}{\bar{S}_f} \right)^* \end{aligned} \quad (A6)$$

where \bar{S}_f is complex power at the fundamental frequency; \dot{V}_f is the fundamental voltage phasor. Based on the above modeling process, the main parameters of the system at the harmonic frequency can be determined. Finally, the nodal admittance matrix Y_h under the harmonic condition is obtained.

References

1. Cui, H.; Wang, C.; Ye, J.; Xue, J.; Yang, B. Research of interaction of distributed PV system with multiple access points and distribution network. *Power Syst. Prot. Control* **2015**, *43*, 91–97.
2. Sun, K.; Qiu, W.; Dong, Y.; Zhang, C.; Yin, H.; Yao, W.; Liu, Y. WAMS-based HVDC Damping Control for Cyber Attack Defense. *IEEE Trans. Power Syst.* **2022**, *38*, 702–713. [[CrossRef](#)]

3. Zhu, C.; Lu, W.; Zhao, W.; Hong, Z.; Chen, C. On-Site energy consumption technologies and prosumer marketing for distributed poverty alleviation photovoltaic linked to agricultural loads in China. *IEEE Access* **2020**, *8*, 191561–191573. [CrossRef]
4. Kouro, S.; Leon, J.I.; Vinnikov, D.; Franquelo, L.G. Grid-Connected Photovoltaic Systems: An Overview of Recent Research and Emerging PV Converter Technology. *IEEE Ind. Electron.* **2015**, *9*, 47–61. [CrossRef]
5. Aydin, M.S.; Alnaser, S.W.; Althaher, S.Z. Using OLTC-Fitted Distribution Transformer to Increase Residential PV Hosting Capacity: Decentralized Voltage Management Approach. *Energies* **2022**, *15*, 4836. [CrossRef]
6. Chen, W.; Ai, X.; Wu, T.; Liu, H. Influence of grid-connected photovoltaic system on power network. *Electr. Power Autom. Equip.* **2013**, *33*, 26–32+39.
7. Sun, K.; Li, K.; Zhang, Z.; Liang, Y.; Liu, Z.; Lee, W.-J. An Integration Scheme of Renewable Energies, Hydrogen Plant, and Logistics Center in the Suburban Power Grid. *IEEE Ind. Appl.* **2022**, *58*, 2771–2779. [CrossRef]
8. Alnaser, S.; Ochoa, L.N. Final Report for WP 1.1 and 1.2 Wide-Scale Adoption of PV in UK Distribution Networks. 2017. Available online: https://www.researchgate.net/publication/313038816_Final_Report_for_WP_11_and_12_Wide-Scale_Adoption_of_PV_in_UK_Distribution_Networks (accessed on 27 May 2022).
9. Hu, X.; Wang, L.; Gong, C.; Xiao, L.; Chen, X. Harmonic analysis and suppression strategies of grid current for renewable energy grid integration system. *Proc. CSEE* **2010**, *30*, 167–170.
10. Makram, E.B.; Thompson, R.L.; Girgis, A.A. A new laboratory experiment for transformer modeling in the presence of harmonic distortion using a computer controlled harmonic generator. *IEEE Trans. Power Syst.* **1988**, *3*, 1857–1863. [CrossRef]
11. Ayres, H.M.; Salles, D.; Freitas, w. A Practical Second-Order Based Method for Power Losses Estimation in Distribution Systems With Distributed Generation. *IEEE Trans. Power Syst.* **2014**, *29*, 666–674. [CrossRef]
12. Quezada, V.H.M.; Abbad, J.R.; Roman, T.G.S. Assessment of energy distribution losses for increasing penetration of distributed generation. *IEEE Trans. Power Syst.* **2006**, *21*, 533–540.
13. Alqatamin, M.; McIntyre, M.L. Nonlinear Self-Synchronizing Current Control for Grid-Connected Photovoltaic Inverters. *Energies* **2022**, *15*, 4855. [CrossRef]
14. Shen, Y.; Liu, J.; Zhang, B.; Liang, L. Research on dynamic harmonic equivalent modeling and influencing factors of photovoltaic inverter. *Proc. CSU-EPSSA* **2019**, *31*, 126–132.
15. Xu, D.; Wang, F.; Mao, H.; Ruan, Y.; Zhang, W. Modeling and analysis of harmonic interaction between multiple grid-connected inverters and the utility grid. *Proc. CSEE* **2013**, *33*, 64–71.
16. Li, Y.; Sun, K.; Li, K.; Sun, K.; Liu, Z.; Xu, Q. Harmonic Modeling of the Series-Connected Multi-Pulse Rectifiers Under Unbalanced Conditions. *IEEE Ind. Electron.* **2022**, *70*, 6494–6505. [CrossRef]
17. Liang, X.; Andalib-Bin-Karim, C. Harmonics and mitigation techniques through advanced control in grid-connected renewable energy sources: A review. *IEEE Trans. Ind. Appl.* **2018**, *54*, 3100–3111. [CrossRef]
18. Rezkallah, M.; Chandra, A.; Hamadi, A.; Ibrahim, H.; Ghandour, M. Power Quality in Smart Grids. In *Pathways to a Smarter Power System*; Elsevier: London, UK, 2019.
19. Wang, X.; Zhao, L.; Lu, K.; Lin, Q.; Wang, P. Calculation of transformer loss and insulation life under harmonic currents. *Proc. CSU-EPSSA* **2016**, *28*, 79–82.
20. Li, Y.; Sun, Y.; Wang, Q.; Sun, K.; Li, K.; Zhang, Y. Probabilistic harmonic forecasting of the distribution system considering time-varying uncertainties of the distributed energy resources and electrical loads. *Appl. Energy* **2022**, *329*, 120298. [CrossRef]
21. Hu, M.; Chen, Y. Survey of power quality and its analysis method. *Power Syst. Technol.* **2000**, *24*, 36–38.
22. Tonini, L.G.R.; Ferraz, R.S.F.; Batista, O.E. Load Flow and Short-Circuit Methods for Grids Dominated by Inverter-Based Distributed Generation. *Energies* **2022**, *15*, 4723. [CrossRef]
23. Sun, Y.; Wang, X.; Yin, Z. Non-iterative harmonic power flow analysis for power systems with multiple harmonic sources. *Proc. CSEE* **2012**, *32*, 83–90.
24. Yong, J.; Chen, L.; Chen, S. Frequency domain harmonic model and attenuation characteristics of desktop PC loads. *Proc. CSEE* **2010**, *30*, 122–129.
25. Chang, G.; Hatziaadoniu, C.H.; Xu, W.; Ribeiro, P.; Burch, R.; Grady, W.; Halpin, M.; Renade, S.; Ruthman, D.; Watson, N.; et al. Modeling devices with nonlinear Voltage-current Characteristics for harmonic studies. *IEEE Trans. Power Deliv.* **2004**, *19*, 1802–1811. [CrossRef]
26. Smith, B.C.; Arrillaga, J.; Wood, A.R.; Watson, N.R. A review of iterative harmonic analysis for AC-DC power systems. *IEEE Trans. Power Deliv.* **1998**, *13*, 180–185. [CrossRef]
27. Ambriz-Perez, H.; Acha, E.; Fuerte-Esquivel, C.R. Advanced SVC models for Newton-Raphson load flow and Newton optimal power flow studies. *IEEE Trans. Power Syst.* **2000**, *15*, 129–136. [CrossRef]
28. Chen, H.; Liao, P. Computation method of harmonic power flow via reducing dimension. *Autom. Electr. Power Syst.* **1996**, *20*, 20–22.
29. Bonner, A.; Grebe, T.; Gunther, E.; Hopkins, L.; Man, M.; Mahseredjian, J.; Miller, N.; Ortmeyer, T.; Rajagopalan, V.; Ranade, S.; et al. IEEE Harmonics Model. Simulation Task Force. Modelling and simulation of the propagation of harmonics in electric power networks: Part I. *IEEE Trans. Power Deliv.* **1996**, *11*, 452–465.
30. Ghorbani, M.J.; Mokhtari, H. Impact of Harmonics on Power Quality and losses in Power Distribution Systems. *Int. J. Electr. Comput. Eng.* **2015**, *7*, 166–174. [CrossRef]

31. Li, Q.; Zhou, L.; Liu, H.; Cui, X.; Zhang, Z.; Fei, S. Simulation calculation and experimental research on harmonic losses in power transformers. *Power Syst. Technol.* **2013**, *37*, 3521–3527.
32. Eason, G.; Noble, B.; Sneddon, I.N. On certain integrals of Lipschitz-Hankel type involving products of Bessel functions. *Phil. Trans. Roy. Soc. Lond.* **1995**, *247*, 529–551.
33. Tofoli, F.L.; Sanhueza, S.M.R.; de Oliveira, A. On the study of losses in cables and transformers in nonsinusoidal conditions. *IEEE Trans. Power Deliv.* **2006**, *21*, 971–978. [[CrossRef](#)]
34. Fang, X.; Yang, Q.; Yan, W. Power generation maximization of distributed photovoltaic systems using dynamic topology reconfiguration. *Prot. Control Mod. Power Syst.* **2022**, *7*, 35. [[CrossRef](#)]
35. Dabra, V.; Paliwal, K.K.; Sharma, P.; Kumar, N. Optimization of photovoltaic power system: A comparative study. *Prot. Control Mod. Power Syst.* **2017**, *2*, 3. [[CrossRef](#)]
36. JCS. Calculation Method of Carrying Capacity of Bare Wire. JCS 0374, 2003. Available online: <https://www.jcma2.jp/jcs/kikaku/index.html> (accessed on 20 December 2022).
37. Fuchs, E.F.; Yildirim, D.; Grady, W.M. Measurement of eddy-current loss coefficient P_{EC-R} , derating of single-phase transformers, and comparison with K-factor approach. *IEEE Trans. Power Deliv.* **2000**, *15*, 148–154. [[CrossRef](#)]
38. *IEEE Std C57.110*; Anonymous Recommended Practice for Establishing Transformer Capability When Supplying Nonsinusoidal Load Currents. IEEE: Piscataway, NJ, USA, 1998.
39. Duan, H.; Jin, D.; Ji, X. Optimization method for selection of distribution transformer based on theory of loss reduction. *Proc. CSU-EPSA* **2015**, *27*, 43–47.
40. Baran, M.E.; Wu, F.F. Network reconfiguration in distribution systems for loss reduction and load balancing. *IEEE Trans. Power Deliv.* **1989**, *4*, 1401–1407. [[CrossRef](#)]

Disclaimer/Publisher’s Note: The statements, opinions and data contained in all publications are solely those of the individual author(s) and contributor(s) and not of MDPI and/or the editor(s). MDPI and/or the editor(s) disclaim responsibility for any injury to people or property resulting from any ideas, methods, instructions or products referred to in the content.